Possible Phases of the Two-Dimensional $t - t'$ Hubbard Model

V. Hankevych[1,2] and F. Wegner[1]

[1]*Institut für Theoretische Physik, Universität Heidelberg, Philosophenweg 19, D-69120 Heidelberg, Germany*
[2]*Department of Physics, Ternopil State Technical University, 56 Rus'ka St., UA-46001 Ternopil, Ukraine*
(Dated: February 1, 2008)

We present a stability analysis of the 2D $t - t'$ Hubbard model on a square lattice for various values of the next-nearest-neighbor hopping t' and electron concentration. Using the free energy expression, derived by means of the flow equations method, we have performed numerical calculation for the various representations under the point group $C_{4\nu}$ in order to determine at which temperature symmetry broken phases become more favorable than the symmetric phase. A surprisingly large number of phases has been observed. Some of them have an order parameter with many nodes in **k**-space. Commonly discussed types of order found by us are antiferromagnetism, $d_{x^2-y^2}$-wave singlet superconductivity, d-wave Pomeranchuk instability and flux phase. A few instabilities newly observed are a triplet analog of the flux phase, a particle-hole instability of p-type symmetry in the triplet channel which gives rise to a phase of magnetic currents, an s^*-magnetic phase, a g-wave Pomeranchuk instability and the band splitting phase with p-wave character. Other weaker instabilities are found also. A comparison with experiments is made.

I. INTRODUCTION

In recent years the two-dimensional (2D) Hubbard model has been used [1, 2] as the simplest model which maps the electron correlations in the copper-oxide planes of high-temperature superconductors since experimental data suggest that superconductivity in cuprates basically originates from the CuO_2 layers [3]. Although in the high-temperature cuprate superconductors electron-electron interactions are strong some important features of these systems (in particular, antiferromagnetic and d-wave superconducting instabilities) are captured already by the 2D Hubbard model at weak to moderate Coulomb coupling.

Apart from the antiferromagnetism and $d_{x^2-y^2}$-wave superconductivity above mentioned (for review see [2, 4] and references therein), a few other instabilities related to symmetry-broken states [5, 6, 7, 8, 9, 10, 11, 12, 13, 14], and truncation of the Fermi surface [15] in the 2D $t - t'$ Hubbard model with next-nearest-neighbor hopping t' have been reported. One of these phases is the staggered flux phase of singlet type with d-wave character which occurs in the particle-hole channel and breaks translational and time-reversal symmetries. The singlet flux phase has been discovered in the mean-field treatments of the 2D Hubbard model by Kotliar [5], and independently by Affleck and Marston [6]. It has been discussed by Nayak [16] and Chakravarty et al. [17] as a d-density wave state which may coexist with d-wave superconductivity. Recently, a triplet analog of the staggered flux phase has been observed [14] also in the 2D $t - t'$ Hubbard model in certain regions of the parameters.

Another instability in the 2D $t - t'$ Hubbard model is a d-wave Pomeranchuk instability breaking the tetragonal symmetry of the Fermi surface, i.e. a spontaneous deformation of the Fermi surface reducing its symmetry to orthorhombic. It has been recently observed for small values of t' from renormalization group calculations by Halboth and Metzner [7]. They argued that the Pomeranchuk instability occurs more easily if the Fermi surface is close to the saddle points of the single particle dispersion (Van Hove filling) with a sizable t' (reducing nesting which leads to antiferromagnetism). However, within their technique it is difficult to compare the strength of the Fermi surface deformation with other instabilities and to conclude which one dominates. The authors of Ref. [12] have investigated the interplay of d-density wave and Fermi surface deformation tendencies with those towards d-wave pairing and antiferromagnetism by means of a similar temperature-flow renormalization group approach. They have found that the d-wave Pomeranchuk instability is never dominant in the 2D $t - t'$ Hubbard model (even under the conditions mentioned above). At the same time, the $d_{x^2-y^2}$-wave Pomeranchuk instability has been observed [13] to be one of the strongest instability in the 2D Hubbard model by means of the flow equations method, but these calculations have some limitations at low temperatures (see Section II).

On the other hand, Vollhardt et al. [18] showed that t'-hopping destroys antiferromagnetic nesting instability at weak interactions in two and three dimensions, and supports the stabilization of metallic ferromagnetism in infinite dimensions away from half-filling. Therefore, one may expect also the stabilization of ferromagnetism by a sizable t' in two dimensions. Indeed, in the $t - t'$ Hubbard model on a 2D square lattice at week to moderate Coulomb coupling, a projection quantum Monte Carlo calculation with 20×20 sites and the T-matrix technique [9], a generalized random phase approximation including particle-particle scattering [8] point towards a ferromagnetic ground state for large negative values of t' in a density range around the Van Hove filling. Similar tendencies have been found

by the authors of Ref. [10] within the renormalization group and parquet approaches. Honerkamp and Salmhofer recently studied [11] the stability of this ferromagnetic region at finite temperatures by means of the temperature-flow renormalization group technique. They have found that ferromagnetic instability is the leading one at $t' < -0.33t$ and the Van Hove filling with critical temperatures depending on the value of t'. When the electron concentration is increased slightly above the Van Hove filling, the ferromagnetic tendencies get cut off at low temperatures and a triplet p-wave superconducting phase dominates. However, they did not consider the Pomeranchuk instability and other ones apart from antiferromagnetism, d- and p-wave superconductivity and ferromagnetism.

Other instabilities recently found in the 2D Hubbard model are an "insulating spin liquid state" [15] and "band splitting" phase [13]. Insulating spin liquid phase is the state with truncated Fermi surface and unbroken translational symmetry. It is insulating due to the vanishing local charge compressibility, and a spin liquid because of the spin gap arising from the pairing correlations. Band splitting phase is a particle-hole instability of singlet type with p-type symmetry which has been found [13] close to half-filling. It leads to a splitting into two bands, and may lead to an energy gap in the charge excitations spectrum.

In the present paper, which is the continuation and extended version of our previous work [14], we investigate the possible phases of the 2D $t - t'$ Hubbard model on a square lattice with the help of the free energy expressions derived in Ref. [13] by means of the flow equations method. In addition to the short paper [14] we present a summary of the formalism, and give some details of numerical calculations as well as consider the case of arbitrary electron concentrations. The phases found by us are discussed in more details. We find all commonly discussed states as well as a few new possible phases. We determine in which regions various symmetry broken phases are more favorable than the symmetric (i.e. normal) state. This is done for various types of symmetry breaking independently, that is if no other symmetry breaking would be present. One phase may suppress another phase. To which extend two order parameters can coexist with each other is a question, which has to be investigated in the future. The paper has the following structure. In Section II we summarize the formalism, and represent the details of numerical calculations. In Section III the numerical results of our stability analysis are given, and the possible phases of the model are discussed. Section IV is devoted to the conclusions.

II.   FORMALISM AND NUMERICS

We consider the $t - t'$ Hubbard model

$$H = \sum_{\mathbf{k}\sigma} \varepsilon_{\mathbf{k}} c_{\mathbf{k}\sigma}^{\dagger} c_{\mathbf{k}\sigma} + \frac{1}{N} \sum_{\substack{\mathbf{k}_1 \mathbf{k}_1' \\ \mathbf{k}_2 \mathbf{k}_2'}} V(\mathbf{k}_1, \mathbf{k}_2, \mathbf{k}_1', \mathbf{k}_2') c_{\mathbf{k}_1\uparrow}^{\dagger} c_{\mathbf{k}_1'\uparrow} c_{\mathbf{k}_2\downarrow}^{\dagger} c_{\mathbf{k}_2'\downarrow}, \tag{1}$$

where $\varepsilon_{\mathbf{k}}$ is the Bloch electron energy with the momentum $\mathbf{k}$, $c_{\mathbf{k}\sigma}^{\dagger} (c_{\mathbf{k}\sigma})$ is the creation (annihilation) operator for the electrons with spin projection $\sigma \in \{\uparrow, \downarrow\}$, and initially $V(\mathbf{k}_1, \mathbf{k}_2, \mathbf{k}_1', \mathbf{k}_2') = U\delta_{\mathbf{k}_1 + \mathbf{k}_2, \mathbf{k}_1' + \mathbf{k}_2'}$ is the local Coulomb repulsion of two electrons of opposite spins, N is the number of lattice points, lattice spacing equals unity.

For a square lattice the single particle dispersion has the form

$$\varepsilon_{\mathbf{k}} = -2t(\cos k_x + \cos k_y) - 4t' \cos k_x \cos k_y, \tag{2}$$

where t is the hopping integral of electrons between nearest neighbors of the lattice, and t' is the next-nearest-neighbor hopping integral. The spectrum (2) contains Van Hove singularities in the density of states at the energy $\varepsilon_{VH} = 4t'$ related to the saddle points of the Fermi surface at $\mathbf{k} = (0, \pm\pi)$ and $(\pm\pi, 0)$. For $t' = 0$ and half-filling the Fermi surface is nested $\varepsilon_{\mathbf{k}+\mathbf{Q}} = -\varepsilon_{\mathbf{k}}$ with $\mathbf{Q} = (\pi, \pi)$, which leads to an antiferromagnetic instability for $U > 0$. The nesting is removed for $t'/t \neq 0$.

We are mainly interested in the following channels

$$V_B(\mathbf{k}, \mathbf{q}) = V(\mathbf{k}, -\mathbf{k}, \mathbf{q}, -\mathbf{q}), \tag{3}$$

$$V_H(\mathbf{k}, \mathbf{q}) = V(\mathbf{k}, \mathbf{q}, \mathbf{k}, \mathbf{q}), \tag{4}$$

$$V_F(\mathbf{k}, \mathbf{q}) = V(\mathbf{k}, \mathbf{q}, \mathbf{q}, \mathbf{k}), \tag{5}$$

$$V_A(\mathbf{k}, \mathbf{q}) = V(\mathbf{k}, \mathbf{q} + \mathbf{Q}, \mathbf{q}, \mathbf{k} + \mathbf{Q}), \tag{6}$$

$$V_C(\mathbf{k}, \mathbf{q}) = V(\mathbf{k}, \mathbf{q} + \mathbf{Q}, \mathbf{k} + \mathbf{Q}, \mathbf{q}), \tag{7}$$

$$V_Y(\mathbf{k}, \mathbf{q}) = V(\mathbf{k}, \mathbf{Q} - \mathbf{k}, \mathbf{q}, \mathbf{Q} - \mathbf{q}). \tag{8}$$

V_B describes the coupling of electron-pairs, V_H and V_F are interactions showing up in Fermi-liquid theory and describe (homogeneous) magnetism and Pomeranchuk-instabilities, channels V_A and V_C describe antiferromagnetism

TABLE I: The factors $\varepsilon_\mathbf{a}, \varepsilon_\mathbf{b}$, and $\mathbf{r}$ in Eq. 10

i	$\varepsilon_\mathbf{a}$	$\varepsilon_\mathbf{b}$	$\mathbf{r}$
B	$\varepsilon_\mathbf{k} - \varepsilon_\mathbf{q}$	$\varepsilon_\mathbf{q} - \varepsilon_\mathbf{k}$	$\mathbf{k} + \mathbf{q}$
F	$\varepsilon_\mathbf{k} + \varepsilon_\mathbf{q}$	$\varepsilon_\mathbf{k} + \varepsilon_\mathbf{q}$	$\mathbf{k} + \mathbf{q}$
H	$\varepsilon_\mathbf{k} - \varepsilon_\mathbf{q}$	$\varepsilon_\mathbf{k} - \varepsilon_\mathbf{q}$	$\mathbf{k} - \mathbf{q}$
A	$\varepsilon_\mathbf{k} + \varepsilon_{\mathbf{q}+\mathbf{Q}}$	$\varepsilon_{\mathbf{k}+\mathbf{Q}} + \varepsilon_\mathbf{q}$	$\mathbf{k} + \mathbf{q} + \mathbf{Q}$
C	$\varepsilon_\mathbf{k} - \varepsilon_\mathbf{q}$	$\varepsilon_{\mathbf{k}+\mathbf{Q}} - \varepsilon_{\mathbf{q}+\mathbf{Q}}$	$\mathbf{k} - \mathbf{q}$
Y	$\varepsilon_\mathbf{k} - \varepsilon_{\mathbf{Q}-\mathbf{q}}$	$\varepsilon_\mathbf{q} - \varepsilon_{\mathbf{Q}-\mathbf{k}}$	$\mathbf{k} + \mathbf{q} - \mathbf{Q}$

and charge density waves with wave-vector $\mathbf{Q}$ as well as some other types of ordering. V_Y describes electron pairs with wave-vector $\mathbf{Q}$. These channels are kept within our approach, but finally the effective interaction V_Y is rather weak. We apply the flow equation method [19, 20] to this Hamiltonian, that is we perform a continuous unitary transformation as a function of a flow parameter l which brings the Hamiltonian into a mean-field form,

$$\frac{dH(l)}{dl} = [\eta(l), H(l)], \quad \eta(l) = [H(l), H^\mathrm{r}(l)]. \tag{9}$$

$\eta(l)$ is the generator of the unitary transformation. $H^\mathrm{r}(l)$ is obtained from the interaction part of the transformed Hamiltonian $H(l)$ by $V^\mathrm{r}(\mathbf{k}_1, \mathbf{k}_2, \mathbf{k}_1', \mathbf{k}_2', l) = r_\mathrm{eli}(\mathbf{k}_1, \mathbf{k}_2, \mathbf{k}_1', \mathbf{k}_2')V(\mathbf{k}_1, \mathbf{k}_2, \mathbf{k}_1', \mathbf{k}_2', l)$, where r_eli is the elimination factor which indicates how urgently $V(\mathbf{k}_1, \mathbf{k}_2, \mathbf{k}_1', \mathbf{k}_2', l)$ should be eliminated. We choose $r_\mathrm{eli}(\mathbf{k}_1, \mathbf{k}_2, \mathbf{k}_1', \mathbf{k}_2') = \sum_\alpha (v_{\mathbf{k}_1}^\alpha + v_{\mathbf{k}_2}^\alpha - v_{\mathbf{k}_1'}^\alpha - v_{\mathbf{k}_2'}^\alpha)^2$ with $v_\mathbf{k}^\alpha = -v_{-\mathbf{k}}^\alpha = v_{\mathbf{k}+\mathbf{Q}}^\alpha$. This condition guarantes, that those interactions we wish to keep have $r_\mathrm{eli} = 0$ and are kept, but the other ones have $r_\mathrm{eli} > 0$ and thus will be eliminated. In this way we eliminate the fluctuations around the molecular-field type behavior and keep finally an interaction for which the molecular-field treatment is exact.

Keeping these interactions in second order in the Hubbard coupling U by means of the flow equation method [20] the Hamiltonian is transformed into an effective one of molecular-field type which contains products of the biquadratic terms $c^\dagger c$, $c^\dagger c^\dagger$, and cc with total momenta 0 and $\mathbf{Q}$, and depends only on two independent momenta. The second order effective interactions are $V_B^{(2)} = W_B$, $V_F^{(2)} = W_F$, $V_H^{(2)} = V_F^{(2)} + W_H$, $V_A^{(2)} = W_A$, $V_C^{(2)} = V_A^{(2)} + W_C$, $V_Y^{(2)} = W_Y$, with

$$W_i = -\frac{U^2}{N} \sum_{\mathbf{p_1 p_2}} \frac{(\hat{n}_{\mathbf{p_2}} - n_{\mathbf{p_1}})(\varepsilon_{\mathbf{p_2}} + \hat{\varepsilon}_{\mathbf{p_1}} - [\varepsilon_\mathbf{a} + \varepsilon_\mathbf{b}]/2)}{(\varepsilon_{\mathbf{p_2}} + \hat{\varepsilon}_{\mathbf{p_1}} - [\varepsilon_\mathbf{a} + \varepsilon_\mathbf{b}]/2)^2 + 1/4(\varepsilon_\mathbf{a} + \varepsilon_\mathbf{b})^2} \delta_{\mathbf{p_1}+\mathbf{p_2},\mathbf{r}}, \tag{10}$$

where $i = B, F, H, A, C, Y$, $n_\mathbf{k}$ is the Fermi distribution function, $\hat{n}_{\mathbf{p_2}} = 1 - n_{\mathbf{p_2}}$, $\hat{\varepsilon}_{\mathbf{p_1}} = \varepsilon_{\mathbf{p_1}}$ for $i = F, A$, and $\hat{n}_{\mathbf{p_2}} = n_{\mathbf{p_2}}$, $\hat{\varepsilon}_{\mathbf{p_1}} = -\varepsilon_{\mathbf{p_1}}$ for $i = B, H, C, Y$ respectively [13]. The factors $\varepsilon_\mathbf{a}, \varepsilon_\mathbf{b}$, and $\mathbf{r}$ are listed in table I. Then, the free energy has the form

$$\beta F = \frac{1}{N} \sum_{\mathbf{kq}} \beta U \left(v_1 + \frac{U}{t} V_{\mathbf{k},\mathbf{q}}\right) \Delta_\mathbf{k}^* \Delta_\mathbf{q} + \sum_\mathbf{k} f_\mathbf{k} \Delta_\mathbf{k}^* \Delta_\mathbf{k} = \sum_{\mathbf{kq}} \left(\frac{U}{t} A_{\mathbf{k},\mathbf{q}} + \frac{U^2}{t^2} B_{\mathbf{k},\mathbf{q}} + \delta_{\mathbf{k},\mathbf{q}}\right) \sqrt{f_\mathbf{k}} \Delta_\mathbf{k}^* \sqrt{f_\mathbf{q}} \Delta_\mathbf{q}, \tag{11}$$

where the first term of the middle part of Eq. (11) is the energy contribution and the second term is the entropy contribution, and

$$A_{\mathbf{k},\mathbf{q}} = \frac{v_1 \beta t}{N \sqrt{f_\mathbf{k} f_\mathbf{q}}}, \qquad B_{\mathbf{k},\mathbf{q}} = \frac{\beta t V_{\mathbf{k},\mathbf{q}}}{N \sqrt{f_\mathbf{k} f_\mathbf{q}}}, \tag{12}$$

with $\beta = 1/(k_B T)$, T is the temperature, $V_{\mathbf{k},\mathbf{q}}$ is effective second-order interaction (the factor U^2/t has been extracted from it), $v_1 = \pm 1$ is the sign with which the first order contribution enters into the effective interaction, $f_\mathbf{k}$ is an entropy coefficient, and $\Delta_\mathbf{k}$ are the order parameters. For example, $\langle c_{\mathbf{k}\sigma} c_{-\mathbf{k}\sigma'} \rangle = (\sigma_y)_{\sigma\sigma'} \Delta_\mathbf{k}^s + \sum_\alpha (\sigma_y \sigma_\alpha)_{\sigma\sigma'} \Delta_\mathbf{k}^{t\alpha}$, where σ_α is a Pauli spin matrix ($\alpha = x, y, z$), and $\Delta_\mathbf{k}^s$ ($\Delta_\mathbf{k}^{t\alpha}$) is the singlet (triplet) amplitude. An expression similar to Eq. (11) is obtained for particle-hole channels with the order parameters ν instead of Δ. In this case, for example, we have $\langle c_{\mathbf{k}\sigma}^\dagger c_{\mathbf{k}+\mathbf{Q}\sigma'} \rangle = \nu_\mathbf{k}^s \delta_{\sigma,\sigma'} + \sum_\alpha \nu_\mathbf{k}^{t\alpha} (\sigma_\alpha)_{\sigma\sigma'}$.

In total we consider four channels, two particle-hole and two particle-particle ones, since the total momentum can be 0 and $\mathbf{Q}$. In all cases we distinguish between singlet and triplet excitations, and in the channels corresponding to the total momentum $\mathbf{Q}$ we distinguish also between $\Delta_{\mathbf{k}+\mathbf{Q}} = \pm\Delta_\mathbf{k}$ and $\nu_{\mathbf{k}+\mathbf{Q}} = \pm\nu_\mathbf{k}$ respectively. Therefore, we introduce the following notations: ph denotes particle-hole channel, si (tr) denotes singlet (triplet), $q_\pm$ corresponds to $\Delta_{\mathbf{k}+\mathbf{Q}} = \pm\Delta_\mathbf{k}$ and $\nu_{\mathbf{k}+\mathbf{Q}} = \pm\nu_\mathbf{k}$ respectively, otherwise 0.

In Eq. (11) and the analogous expressions for particle-hole channels one has

channel	v_1	$V_{\mathbf{k},\mathbf{q}}$	$f_{\mathbf{k}}$
$pp\ si/tr\ 0$	$+1$	$V_B^{(2)}(\mathbf{k},\mathbf{q})$	$f(\beta(\varepsilon_{\mathbf{k}}-\mu), \beta(\mu-\varepsilon_{\mathbf{k}}))$
$ph\ si\ 0$	$+1$	$2V_H^{(2)}(\mathbf{k},\mathbf{q})-V_F^{(2)}(\mathbf{k},\mathbf{q})$	$f(\beta(\varepsilon_{\mathbf{k}}-\mu), \beta(\varepsilon_{\mathbf{k}}-\mu))$
$ph\ tr\ 0$	-1	$-V_F^{(2)}(\mathbf{k},\mathbf{q})$	$f(\beta(\varepsilon_{\mathbf{k}}-\mu), \beta(\varepsilon_{\mathbf{k}}-\mu))$
$pp\ si/tr\ q_\pm$	$+1$	$V_Y^{(2)}(\mathbf{k},\mathbf{q})$	$f(\beta(\varepsilon_{\mathbf{k}}-\mu), \beta(\mu-\varepsilon_{\mathbf{k}+\mathbf{Q}}))$
$ph\ si\ q_\pm$	$+1$	$2V_C^{(2)}(\mathbf{k},\mathbf{q})-V_A^{(2)}(\mathbf{k},\mathbf{q})$	$f(\beta(\varepsilon_{\mathbf{k}}-\mu), \beta(\varepsilon_{\mathbf{k}+\mathbf{Q}}-\mu))$
$ph\ tr\ q_\pm$	-1	$-V_A^{(2)}(\mathbf{k},\mathbf{q})$	$f(\beta(\varepsilon_{\mathbf{k}}-\mu), \beta(\varepsilon_{\mathbf{k}+\mathbf{Q}}-\mu))$

$$(13)$$

The entropy coefficient function is

$$f(x,y) = \frac{x-y}{e^x - e^y}(e^x + 1)(e^y + 1). \tag{14}$$

We start from the symmetric state and investigate whether this state is stable against fluctuations of the order parameters Δ and ν. As soon as a non-zero Δ or ν yields a lower free energy in comparison with the symmetric state with all vanishing Δ and ν, then the symmetric state is unstable and the system will approach a symmetry broken state. This indicates a phase transition. Of course, one phase may suppress another phase. To which extend two order parameters can coexist with each other is a question, which has to be investigated. But this problem lies outside the scope of the present paper.

We performed numerical calculation on a square lattice with 24×24 points in the Brillouin zone for the various representations under the point group $C_{4\nu} = 4mm$. This group consists of the following symmetry elements: mirror reflections with respect to the x- and y-axes and the lines $y = \pm x$, a fourfold rotation about the axis which is perpendicular to x-y-plane. The representations of the even-parity states are one-dimensional. We denote them by $s_+ = s_1$, $s_- = g = s_{xy(x^2-y^2)}$, $d_+ = d_{x^2-y^2}$, $d_- = d_{xy}$. The odd-parity representation is two-dimensional, here simply denoted by p.

Initially, such numerical calculations have been performed in Refs. [13, 21], but they were sensitive to the lattice size at low temperatures, specially for the particle-hole channels. The main problem is that the wave-vector space contributing essentially to the order parameter is very small at low temperatures as a result of exponential divergence of the entropy coefficients $f_{\mathbf{k}}$. As we consider the stability of the symmetric state with respect to a symmetry broken phase (thus we are interested in small fluctuations of free energy (11) around zero) and the energy contribution to Eq. (11) changes slowly, the entropy contribution has to change slowly also. Rewriting Eq. (11) in terms of new renormalized order parameter $\tilde{\Delta}_{\mathbf{k}} = \sqrt{f_{\mathbf{k}}}\Delta_{\mathbf{k}}$, we conclude that the averaging $\langle \frac{1}{f_{\mathbf{k}}} \rangle$ has to be performed in $\mathbf{k}$-space when we are calculating entropy coefficients. For the value of the inverse entropy coefficient $1/f_{\mathbf{k_0}}$ we take the average value of the coefficients over $N_a \times N_a$ lattice points of a grid with center at the $\mathbf{k_0}$-point and the spacing $2\pi/(N_a\sqrt{N})$. The number N_a of points in momentum space is inversely proportional to temperature and $\sqrt{N}$, all together these points cover the Brillouin zone. A similar procedure is applied to the chemical potential calculation. One should also perform the averaging in determination of effective interactions, but it would take much more time. We have checked the size effects in the framework of such an improved scheme, performing some calculations also for 16×16 and 32×32 lattices, and found that the differences are very small and unessential. Although size effects increase at low temperatures in the low density region, they do not touch and change the leading instabilities essentially.

For each channel the eigenvalues of the matrix $\frac{U}{t}A + \frac{U^2}{t^2}B$ have to be determined. Whenever the lowest eigenvalue λ (i.e. the most negative) equals -1, then a critical T_c/t or $(U/t)_c$ is reached. For the s_+ representation (in case of the effective interactions V_A, V_C, V_Y only for $\nu_{\mathbf{k}+\mathbf{Q}} = +\nu_{\mathbf{k}}$, $\Delta_{\mathbf{k}+\mathbf{Q}} = +\Delta_{\mathbf{k}}$) one has to find the solution by iterating the eigenvalue equation as a function of U/t. In the case of all other representations the A-term does not contribute. Therefore then we determine the lowest eigenvalue λ of the matrix B, and obtain $(U/t)_c = 1/\sqrt{-\lambda}$.

III.   POSSIBLE PHASES OF THE MODEL

We start from $t' = 0$ and half-filling $n = 1$ (see Fig. 1). As expected in this case the leading instability is the antiferromagnetic one, it appears in the $ph\ tr$ channel with q_+ symmetry and s_+ wave character. As we leave half-filling the antiferromagnetism becomes weaker (Fig. 2) and disappears at hole doping $\delta \equiv 1 - n \sim 0.08$. As soon as the system is doped the nesting is reduced, since there are no longer points on the Fermi surface connected by the wave-vector $\mathbf{Q}$ and we observe a reentrant behavior. The second order contribution to the antiferromagnetic channel suppresses antiferromagnetism (at least in the s-channel). Therefore antiferromagnetism disappears at larger values

of U/t. Strong coupling calculations yield a $t - J$-model in which the exchange coupling decreases like $J = 4t^2/U$ for large U. Thus, our observation is remarkable, since we work with a weak-coupling calculation, we obtain at intermediate couplings the same tendency as it is expected at strong interactions although we do not reproduce the Neél temperature behavior $T_c \sim t^2/U$. We take the decrease of the Neél temperature as an indication that the calculation in second order in U yields reasonable results even for intermediate values $U \sim 4t$. For stronger couplings higher order contributions will become important. However, it is of interest to see which instabilities emerge within our approximation for larger values of U/t, since this gives a hint which types of ordering should be investigated for stronger couplings. Therefore, we discuss the phase diagram obtained from the second order calculation also for larger values U/t. It might be also that higher order contributions neglected by us enhance the tendency towards antiferromagnetism, and then it will decay not so rapidly. Nevertheless, we emphasize that already second order calculations give the qualitative description of antiferromagnetism at intermediate couplings. In the latter context, we make a comparison of our results with experimental data on some high-temperature cuprate superconductors and transition metal compounds. As one can see from Fig. 1 antiferromagnetism disappears at the temperature $T \approx 0.1t$. Taking the estimation for the hopping integral $t \approx 0.1 \div 0.3$ eV, which is the realistic values for transition metal and their compounds [22, 23], we obtain the Neél temperatures $T_c = T_N \approx 110 \div 350$ K. These values agree with experimental data on half-filled antiferromagnetic materials [24]. Let us consider also the parent compound La_2CuO_4 of high-T_c cuprate systems $La_{2-x}M_xCuO_4$ (M = Sr, Ba, Ca). It is an antiferromagnetic insulator with the Neél temperature $T_N \sim 300$ K and half-filled d-band [25]. The electronic structure of these systems is considered to be described by the three-band Hubbard model (or $d - p$ model) [25, 26]. Some of the model parameters deduced from photoemission and LDA calculations are $U_{dd} \approx 6 \div 10$ eV, and $t_{pd} \approx 1 \div 1.5$ eV [25]. The main features of the three-band Hubbard model can be mapped onto the single-band Hubbard model, and therefore one may describe [2] these compounds by the Hubbard model (1). The values of the parameters U and t of such a single-band Hubbard model are smaller in comparison with the corresponding parameters U_{dd} and t_{pd} of the three-band extended Hubbard model, the Coulomb repulsion U is specially reduced [27]. Then, taking the values $t \approx 1$ eV and $U/t \approx 4.7 \div 4.8$ (it corresponds to $T_c/t \approx 0.03 \div 0.02$) we obtain the theoretical estimation of the Neél temperature for La_2CuO_4 around $T_N \approx 290$ K, that is very close to the experimental value.

The next instability is a Pomeranchuk instability with $d_{x^2-y^2}$-wave symmetry in the singlet channel (namely $ph\ si\ 0$). The corresponding eigenvector signals a deformation of the Fermi surface which breaks the point group symmetry of the square lattice. At high temperatures the system has a tetragonal structure and an orthorhombic one at low temperatures. The $d_{x^2-y^2}$ wave Pomeranchuk instability dominates in the region of temperature $T > 0.05t$ at small hole doping ($\delta < 0.2$), and for negative $t' \geq -t/3$ the Pomeranchuk instability dominates in all temperature region at the electron concentrations around the Van Hove filling (see Figs. 3, 4). It competes with other instabilities at $t' < -t/3$ and the electron concentrations around the Van Hove filling, and it is not the leading one here (Fig. 5). But the d-wave Pomeranchuk instability appears again to dominate at large negative $t' < -t/3$ in the region of electron density above the Van Hove filling and below some doping (for example, see Fig. 6); for the value $t' = -5t/12$ this value of doping equals $\delta \approx 0.2$. In agreement with the ideas of Ref. [7] the instability is mainly driven by a strong attractive interaction between particles on opposite corners of the Fermi surface near the saddle points and a repulsive interaction between particles on neighboring corners. To favor such a behavior we need a sizable t' reducing antiferromagnetic correlations. The critical temperature of the d-wave Pomeranchuk instability occurrence decreases with increasing hole doping, and at sufficiently large values of doping and away from Van Hove filling this phase requires strong couplings. Thus the hole doping suppresses the tendency towards an orthorhombic distortion of the Fermi surface (or lattice). The tendency towards a spontaneous deformation of Fermi surface with d-wave character has been observed by A. P. Kampf and A. A. Katanin [28] to be one of the leading instabilities in the 2D extended U-V-J Hubbard model in the parameter range which is relevant for underdoped cuprate systems. A similar Pomeranchuk instability has been found by the authors of Ref. [29] to be a characteristic of a nematic Fermi fluid [30] in two dimensions.

Another possible phase is a particle-hole instability of singlet type with staggered p-wave symmetry ($ph\ si\ q_-\ p$). The corresponding quasiparticle energy spectrum is

$$E_{\mathbf{k}} = \pm\sqrt{\varepsilon_{\mathbf{k}}^2 + \tilde{\varepsilon}_{\mathbf{k}}^2} \qquad (15)$$

where

$$\tilde{\varepsilon}_{\mathbf{k}} = \frac{1}{N}\sum_{\mathbf{q}}[2V_C(\mathbf{k},\mathbf{q}) - V_A(\mathbf{k},\mathbf{q}) - 2V_C(\mathbf{k},\mathbf{q}+\mathbf{Q}) + V_A(\mathbf{k},\mathbf{q}+\mathbf{Q})]\nu_{\mathbf{q}}^s \qquad (16)$$

varies like $\tilde{\varepsilon}_x \sin k_x + \tilde{\varepsilon}_y \sin k_y$ with roughly constant $\tilde{\varepsilon}_x$ and $\tilde{\varepsilon}_y$. It yields a splitting into two bands and may lead to an energy gap in the charge excitations spectrum. Another mechanism for a charge gap formation has been proposed [31, 32] recently in the 2D Hubbard model with $t' = 0$ at weak coupling. The band splitting phase is developed in the region of electron concentration around half-filling, and is one of the strongest in that region. This

instability dominates when the electron concentration $n > 1.10$ and $t' \neq 0$ (Fig. 7). The negative next-nearest-neighbors hopping favors this phase to be dominant instability at electron doping, but the value of coupling strength U/t required for the occurrence of this instability increases with increasing $|t'|$. The critical temperature of the transition to the band splitting phase decreases with increasing electron doping, thus the electron doping suppresses the tendency towards this phase.

The singlet superconducting $d_{x^2-y^2}$ instability (pp si 0 d_+) coincides with the $d_{x^2-y^2}$-wave staggered flux phase at half-filling and $t' = 0$ (the discussion on flux phases appears in the next paragraph). Away from half-filling the degeneration disappears, and d-wave superconductivity dominates at low temperatures in certain regions of electron concentration around half-filling which depend on the value of $t' \neq 0$. Even large values of $|t'|$ do not destroy the dominant low-temperature behavior of $d_{x^2-y^2}$-wave superconductivity at hole doping (Fig. 4). It is not destroyed also at sufficiently large hole doping: for small $t' \geq -t/6$ even at the values of hole doping $\delta \sim 0.3$, and for $t' \leq -t/3$ at $\delta \sim 0.15$ the d-wave superconductivity dominates at low temperatures. However, this dominant behavior is destroyed around the Van Hove filling where other phases appear to dominate. At small electron doping d-wave superconductivity dominates at low temperatures also, but it is not the leading instability at $n - 1 \geq 0.1$ and $t' \neq 0$ (see Fig. 7). In contrast to the pure 2D Hubbard model with $t' = 0$, an electron-hole asymmetry of the d-wave superconducting phase is manifested in the $t - t'$ Hubbard model. In this model with negative t' the d-wave superconductivity appears to dominate within wider region of hole doping in comparison with the electron doping in agreement with the one-loop renormalization group analysis [33]. In this connection it should be mentioned that the most examples of discovered high-temperature superconducting materials are hole-doped systems, and only a few examples are electron-doped ones.

We observe also particle-hole instabilities with staggered symmetry of d_+ wave character in singlet and triplet channels (ph si/tr q_- d_+). These states are singlet and triplet flux phases which are approximately described by the operators structures

$$i \sum_{\mathbf{k}\sigma} (\cos k_x - \cos k_y) c^\dagger_{\mathbf{k}+\mathbf{Q}\sigma} c_{\mathbf{k}\sigma}, \tag{17}$$

$$i \sum_{\mathbf{k}\sigma\sigma'} (\cos k_x - \cos k_y) \vec{\sigma}_{\sigma\sigma'} c^\dagger_{\mathbf{k}+\mathbf{Q}\sigma} c_{\mathbf{k}\sigma'}, \tag{18}$$

respectively, where the components of $\vec{\sigma}$ are 2×2 spin Pauli matrices. For $t' = 0$ critical temperatures of the transition to the singlet and triplet flux phases are degenerate, in this case these phases vanish at hole doping $\delta \sim 0.12$ in agreement with a mean-field solution of the $t - J$ model presented in Ref. [34]. For $t' \neq 0$ they occur more easily at the electron concentrations which are slightly above the Van Hove filling, but the singlet flux phase disappears for $t' \leq -t/3$. For non-zero values of the next-nearest-neighbors hopping the critical transition temperatures of these phases are different, and the triplet one is higher. Moreover, the triplet analog of flux phase dominates at low temperatures and $t' = -5t/12$ when the electron concentration is slightly above the Van Hove filling (see Fig. 8) in contrast to the results of Ref. [11] which point out the occurrence of triplet superconductivity with p-wave symmetry in this region. The triplet flux phase is also one of the leading instabilities for various values of next-nearest-neighbors hopping t' and certain region of electron concentrations (for example, see Fig. 3, 5, 6).

The singlet flux state, described by Eq. (17), breaks time-reversal, translational, and rotational symmetries. This state is a phase of circular charge currents flowing around the plaquettes of a square lattice with alternating directions. The authors of Ref. [34] found that these currents generate a small magnetic field, also forming a staggered pattern, and they estimated the field strength just above the plaquette center to be around 10 G. They pointed out that muon-spin-rotation experiments may be able to detect this magnetic field. Recently, the idea of circulating orbital currents (also called an orbital antiferromagnetism) has been discussed as promising candidates for a description of the pseudogap phase of high-T_c cuprates [17, 35, 36]. There is also a proposal [37] of a circulating current phase, which does not break translational symmetry. The possible existence of orbital charge currents has most recently received experimental support. Angle-resolved photoemission with circularly polarized light identified intensity differences for left- and right-circularly polarized photons in the psedogap phase of $Bi_2Sr_2CaCu_2O_{8+\delta}$ [38]. Also small c-axis oriented ordered magnetic moments, and an evidence for static alternating magnetic fields below the psedogap temperature in the underdoped $YBa_2Cu_3O_{6+x}$ systems were observed by neutron scattering [39] and muon-spin-rotation [40] measurements respectively. These data can find a natural interpretation in terms of planar circulating current phases [41].

The triplet flux phase, described by Eq. (18), breaks translational, rotational and spin-rotational symmetries, and does not break time-reversal invariance. This phase is a state in which spin-up and spin-down electron currents circulate around the plaquettes in opposite directions to produce non-zero spin currents. It corresponds to an alternating pattern of spin currents. Similar triplet flux phase (so called spin flux phase or spin nematic state) has been discussed by Narsesyan and co-workers [42] by means of a mean-field theory, and more recently in Refs. [28, 43] by means of

renormalization group approaches in the framework of the 2D extended U-V-J Hubbard model. Another triplet flux phase, which breaks time-reversal invariance, has been considered by Nayak [16] as a triplet analog of the density wave order parameter potentially relevant to the cuprates. To our knowledge a triplet version of the flux phase has not yet been observed in numerical solutions of the 2D $t - t'$ Hubbard model. In the case of polarized particle-hole pairs (it means that we take σ_z instead of $\vec{\sigma}$ in Eq. (18)) the alternating pattern of spin currents will generate electric field, which could be, in principle, measurable in experiments. As triplet flux phase (18) does not have anomalous expectation values for the spin density but, rather, for spin currents, these excitations do not contribute to the spin-spin correlation function, therefore spin currents do not couple to photons, neutrons or nuclear spins [16]. However, they could be detected with nuclear quadrupole resonance or two-magnon Raman scattering experiments [16].

At $t' = -5t/12$ a few other new instabilities appear to compete at the Van Hove filling and low temperatures (Fig. 5) in disagreement with the conclusions of Ref. [11] on the occurrence of ferromagnetism. The leading one is another Pomeranchuk instability in the s_+ channel with $g_+ = g_{x^4+y^4-6x^2y^2}$ wave character (ph si 0 s_+, 4 node lines in $\mathbf{k}$-space). This phase occurs more easily when the electron concentration is close to the Van Hove filling, and it is a leading instability at the Van Hove filling and the values of electron concentration which are slightly smaller than the Van Hove filling (Figs. 5, 9). The g_+ Pomeranchuk instability appears at sizable values of next-nearest-neighbors hopping $t' \sim -t/3$ (Fig. 3), but it requests sufficiently large absolute values of t' ($t' < -t/3$) to be one of the dominant instabilities. In the d_- channel an i-wave (6 node lines in $\mathbf{k}$-space) Pomeranchuk instability (ph si 0 d_-) appears when electron concentration n is smaller than the Van Hove filling at $t' = -5t/12$ (Fig. 9). It is a leading one at small values of the electron concentration (Fig. 10), and dominates in the temperature region $T > 0.15t$ at $t = -t'/3$ when the electron concentration is sufficiently below the Van Hove filling. The increase of electron concentration reduces essentially this phase.

When the electron concentration is decreased below the Van Hove density at $t' = -5t/12$, a particle-hole instability of p-wave symmetry in triplet channel (ph tr 0 p) dominates (see Fig. 10). The electron operators structure which describes this magnetic phase is roughly

$$i \sum_{\mathbf{k}\sigma\sigma'} (t_x^M \sin k_x + t_y^M \sin k_y)\vec{\sigma}_{\sigma\sigma'} c_{\mathbf{k}\sigma}^\dagger c_{\mathbf{k}\sigma'} = \frac{i}{2} \sum_{\mathbf{R}\sigma\sigma'} \left(t_x^M [c_{\mathbf{R}+\mathbf{e}_x,\sigma}^\dagger - c_{\mathbf{R}-\mathbf{e}_x,\sigma}^\dagger] + t_y^M [c_{\mathbf{R}+\mathbf{e}_y,\sigma}^\dagger - c_{\mathbf{R}-\mathbf{e}_y,\sigma}^\dagger] \right) \vec{\sigma}_{\sigma\sigma'} c_{\mathbf{R},\sigma'} \quad (19)$$

with $\mathbf{e}_x$ ($\mathbf{e}_y$) being the unit vector along the x- (y-) axis, $\mathbf{R}$ denotes lattice site. The quantity t^M is given by $t_x^M \sin k_x + t_y^M \sin k_y \approx -1/N \sum_{\mathbf{q}} V_F(\mathbf{k}, \mathbf{q})\nu_{\mathbf{q}}^t$. One can see from Eq. (19) that this instability gives rise to a phase of magnetic currents, the magnetization equals zero as a result of p-wave character of the instability. The magnetic currents phase dominates also at very low temperatures and electron concentrations which are slightly smaller the Van Hove filling for $t' = -5t/12$ (Fig. 9), and in the temperature region $T < 0.15t$ below the Van Hove density for $t' = -t/3$.

In the temperature region $T > 0.15t$ a particle-hole instability with s^*-wave character (ph tr 0 s_+, its order parameter changes sign close to the Fermi-edge) in the triplet s_+ channel dominates at $t' \leq -5t/12$ and the density range around the Van Hove filling (see Figs. 5, 8, 9). It is likely that the order parameter contributions do not compensate exactly, so that a weak ferromagnetism appears. When the electron concentration is increased above the Van Hove filling this instability does not become weaker, but the $d_{x^2-y^2}$ wave Pomeranchuk and the triplet flux phase instabilities are stronger and dominate at low temperatures. Then, this s^*-magnetic phase disappears at sufficiently large values of electron concentration in comparison with the Van Hove filling, or smaller $|t'|$. With the decrease of electron concentration from the Van Hove filling this instability becomes weaker and disappears to be a leading one at small electron density (Fig. 10). From Figs. 5, 8, 9 one can see a reentrant behavior of the s^*-magnetic phase in some region of the values U/t: approaching T_c we get T_c^l from low temperatures and T_c^u from high temperatures at the same value of coupling U/t ($T_c^l \neq T_c^u$). This is a result of different behavior of $T_c(U/t)$ in two regimes. First regime occurs in the region where the s^*-magnetic instability dominates and the transition from a paramagnetic state to the s^*-magnetic phase occurs directly without any intermediate phase, it corresponds to the temperatures $T > 0.15t$ in Figs. 5, 9. In this case the critical temperature increases with the increase of correlation strength U/t. Therefore electron correlations enhance the tendency towards the s^*-magnetic instability. Another regime occurs at the temperatures $T < 0.15t$, where the s^*-magnetic phase is not a leading instability and other instabilities dominate. In this situation the critical temperature exhibits an anomalous behavior, it decreases with increasing the coupling U/t. The s^*-magnetic phase is reduced. Since at lower temperatures only a smaller region in $\mathbf{k}$-space around the Fermi-edge contributes, the sign-change of the order parameter reduces the effective interaction. As the transition to this phase requires some finite value of the effective interaction at low temperatures, the correlation strength has to increase rapidly.

We observe also a few other weaker instabilities. Apart from $d_{x^2-y^2}$ wave superconductivity mentioned above other two superconducting instabilities appear. At $t' \leq -t/3$ a d_{xy} wave superconducting phase occurs in the singlet channel sufficiently below the Van Hove filling (see, for example, Fig. 10), and for larger absolute values $t' \leq -5t/12$

we observe a g_+ wave superconductivity in the s_+ singlet channel below the Van Hove filling (Fig. 9). All these phases require strong couplings.

The peculiar feature of the superconducting phase in comparison with the other phases observed by us should be noted. Away from the Van Hove filling when temperature approaches zero the curves corresponding to superconducting phase are flat, whereas the curves corresponding to all other phases observed become steep. Therefore, at very low temperatures the transition from a paramagnetic phase to the superconducting one can occur at very small values of the corresponding effective interaction in contrast with the transitions to other possible phases which require some finite values of the effective interactions. One can see also that the critical temperatures of all phases (excepting antiferromagnetism and s^*-magnetic phase in certain regions) increase with the increase of correlation strength U/t. Thus, electron correlations enhance the tendency towards the transition to the phases observed by us.

IV. CONCLUSIONS

We have presented a stability analysis of the 2D $t - t'$ Hubbard model on a square lattice for various values of the next-nearest-neighbors hopping t' and electron concentration. On the basis of the free energy expression, derived by means of the flow equations method, we have performed numerical calculation for the various representations under the point group $C_{4\nu}$ in order to determine the phase diagram. A surprising large number of phases has been observed. Some of them have an order parameter with many nodes in **k**-space.

For small values of t' and doping the leading instability is the antiferromagnetic one. At $t' = 0$ antiferromagnetism disappears at hole doping $\delta \sim 0.08$ and temperatures $T \sim 0.1t$. This result reproduces the Néel temperatures in some antiferromagnetic materials. The $d_{x^2-y^2}$ wave Pomeranchuk instability dominates in the region of temperature $T > 0.05t$ at small hole doping ($\delta < 0.2$), and for negative $t' \geq -t/3$ the Pomeranchuk instability dominates in all temperature region at the electron concentrations around the Van Hove filling. It is the leading instability at large negative $t' < -t/3$ in the region of electron density above the Van Hove filling and below some doping; for the value $t' = -5t/12$ this value of doping equals $\delta \approx 0.2$. The band splitting phase with staggered p-wave symmetry is developed in the region of electron concentration around half-filling, and is one of the strongest in that region. This instability dominates when the electron concentration $n > 1.10$ and $t' \neq 0$. The negative next-nearest-neighbors hopping favors this phase to be dominant instability at electron doping. The $d_{x^2-y^2}$-wave superconductivity dominates at low temperatures in certain regions of electron concentration around half-filling which depend on the value of $t' \neq 0$. Even large values of $|t'|$ do not destroy the dominant low-temperature behavior of $d_{x^2-y^2}$-wave superconductivity at hole doping. It is not destroyed also at sufficiently large hole doping. However, this dominant behavior is destroyed around the Van Hove filling where other phases appear to dominate. At small electron doping d-wave superconductivity dominates at low temperatures also, but as a result of electron-hole asymmetry of the 2D $t - t'$ Hubbard model the d-wave superconductivity appears to dominate within wider region of hole doping in comparison with the electron doping for negative values of t'. Triplet and singlet flux phases, which have degenerate critical temperatures at $t' = 0$, occur more easily at the electron concentrations which are slightly above the Van Hove filling for $t' \neq 0$. For non-zero values of the next-nearest-neighbors hopping the critical transition temperatures of these phases are different, and the triplet one is higher. The triplet analog of flux phase dominates at low temperatures and $t' = -5t/12$ when the electron concentration is slightly above the Van Hove filling. The triplet flux phase is also one of the leading instabilities for various values of next-nearest-neighbors hopping t' and certain region of electron concentrations. At $t' < -t/3$ and the Van Hove filling the leading instabilities are a g_+ wave Pomeranchuk instability and p-wave particle-hole instability in triplet channel (phase of magnetic currents) at temperatures $T < 0.15t$, and s^*-magnetic phase for $T > 0.15t$. The magnetic currents phase dominates also at very low temperatures and electron concentrations which are slightly smaller the Van Hove filling for $t' = -5t/12$, and in the temperature region $T < 0.15t$ below the Van Hove density for $t' = -t/3$. The s^*-magnetic phase is reduced strongly at low temperatures and shows a reentrant behavior in certain region of U/t. We have found other weaker instabilities also. Most instabilities develop at $U > 4t$, which are not small values. Therefore, flow equation calculations beyond second order would be desirable. Nevertheless, as we have found most commonly discussed types of order, and since some effects obtained in the intermediate to strong couplings are reproduced reasonably well by means of the flow equations, we suggest that our calculations give an estimate of the most important instabilities.

his stay.

[1] Yu. Izyumov, Usp. Fiz. Nauk **42**, 215 (1999).
[2] D.J. Scalapino, Physics Reports **250**, 329 (1995).
[3] For a recent review on the cuprate superconductors see C. C. Tsuei and J. R. Kirtley, Rev. Mod. Phys. **72**, 969 (2000).
[4] W. Hanke *et al.*, Adv. Solid State Phys. **38** (1999).
[5] G. Kotliar, Phys. Rev. B **37**, 3664 (1988).
[6] I. Affleck, J. B. Marston, Phys. Rev. B **37**, 3774 (1988).
[7] C. Halboth and W. Metzner, Phys. Rev. Lett. **85**, 5162 (2000); Phys. Rev. B **61**, 7364 (2000).
[8] M. Fleck, A. M. Oleś, and L. Hedin, Phys. Rev. B **56**, 3159 (1997).
[9] R. Hlubina, S. Sorella, and F. Guinea, Phys. Rev. Lett. **78**, 1343 (1997); Phys. Rev. B **59**, 9600 (1999).
[10] V. Yu. Irkhin, A. A. Katanin, and M. I. Katsnelson, Phys. Rev. B **64**, 165107 (2001).
[11] C. Honerkamp and M. Salmhofer, Phys. Rev. Lett. **87**, 187004 (2001); Phys. Rev. B **64**, 184516 (2001).
[12] C. Honerkamp, M. Salmhofer, and T. M. Rice, Eur. Phys. J. B **27**, 127 (2002).
[13] I. Grote, E. Körding, and F. Wegner, J. Low Temp. Phys. **126**, 1385 (2002).
[14] V. Hankevych, I. Grote, and F. Wegner, Phys. Rev. B **66**, 094516 (2002).
[15] C. Honerkamp, M. Salmhofer, N. Furukawa, and T. M. Rice, Phys. Rev. B **63**, 035109 (2001).
[16] C. Nayak, Phys. Rev. B **62**, 4880 (2000).
[17] S. Chakravarty, R. B. Laughlin, D. K. Morr, and C. Nayak, Phys. Rev. B **63**, 094503 (2001).
[18] D. Vollhardt *et al.*, Adv. Solid State Phys. **35**, 383 (1999).
[19] F. Wegner, Annalen der Physik (Leipzig) **3**, 77 (1994).
[20] For a recent review on the flow equation method see F. Wegner, Physics Reports **348**, 77 (2001).
[21] I. Grote, Ph.D. thesis, University of Heidelberg (2002).
[22] C. Herring, in *Magnetism, Vol. 4*, ed. by G. T. Rao and H. Suhl (Accademic Press, New York, 1966), p. 1.
[23] J. Friedel, in *The Physics of Metals*, ed. by J. M. Ziman (Cambridge University Press, Cambridge, 1969), p. 340.
[24] N. F. Mott, *Metal-Insulator Transition* (Taylor & Francis, London, 1990).
[25] For a review on normal-state properties of high-T_c cuprates see M. Imada, A. Fujimori, and Y.Tokura, Rev. Mod. Phys. **70**, 1039 (1998).
[26] See, for example, P. Fulde, *Electron Correlations in Molecules and Solids*, Springer Ser. Solid-State Sci., Vol. 100 (Springer, Berlin, Heidelberg, 1991), Chap. 14.
[27] F. Wegner (unpublished).
[28] A. P. Kampf and A. A. Katanin, cond-mat/0204542.
[29] V. Oganesyan, S. A. Kivelson, E. Fradkin, Phys. Rev. B **64**, 195109 (2001).
[30] S. A. Kivelson, E. Fradkin, V. J. Emery, Nature **393**, 550 (1998).
[31] S. Moukouri and M. Jarrell, Phys. Rev. Lett. **87**, 167010 (2001).
[32] B. Kyung, J. S. Landry, D. Poulin and A.-M. Tremblay, cond-mat/0112273.
[33] C. Honerkamp, Eur. Phys. J. B **21**, 81 (2001).
[34] T. C. Hsu, J. B. Marston, I. Affleck, Phys. Rev. B **43**, 2866 (1991).
[35] S. Chakravarty, H.-Y. Kee, and C. Nayak, Int. J. Mod. Phys. **15**, 2901 (2001).
[36] P. A. Lee, cond-mat/0201052.
[37] C. M. Varma, Phys. Rev. Lett. **83**, 3538 (1999).
[38] A. Kaminski *et al.*, Nature **416**, 610 (2002).
[39] H. A. Mook *et al.*, Phys. Rev. B **64**, 012502 (2001); **66**, 144513 (2002).
[40] R. I. Miller *et al.* Phys. Rev. Lett. **88**, 137002 (2002).
[41] For a theoretical discussion of the experiments, see Refs. [34, 35] and C. M. Varma, Phys. Rev. B **61**, R3804 (2000).
[42] A. A. Narsesyan, G. I. Japaridze and I. G. Kimeridze, J. Phys.: Condens. Matter **3**, 3353 (1991).
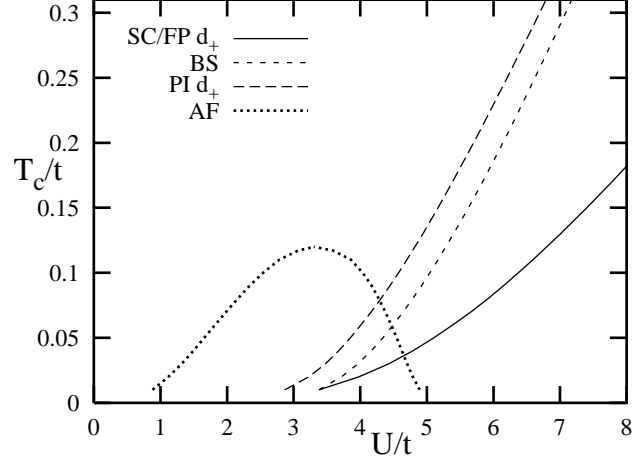[43] B. Binz, D. Baeriswyl, and B. Douçot, Eur. Phys. J. B **25**, 69 (2002).

FIG. 1: Temperature phase diagram of the 2D $t-t'$ Hubbard model for $n=1$, $t'=0$. Chemical potential $\mu=0$. SC stands for superconductivity, FP for flux phase, BS for band splitting, PI for Pomeranchuk instability, AF for antiferromagnetism.
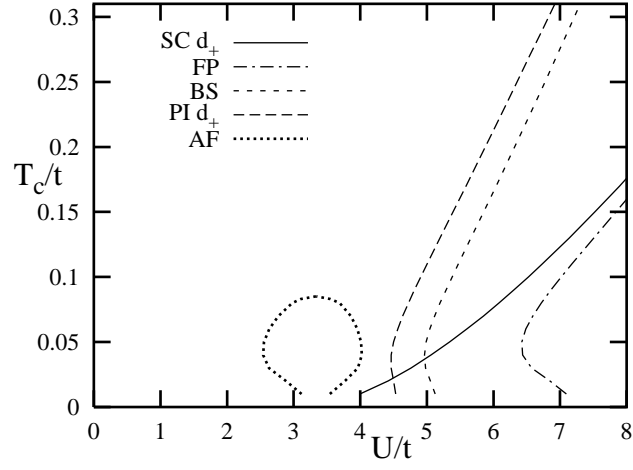

FIG. 2: Temperature phase diagram of the 2D $t-t'$ Hubbard model for $n=0.94$, $t'=0$. Chemical potential varies between $\mu/t = -(0.097 \div 0.146)$. Notations are the same as in Fig. 1.
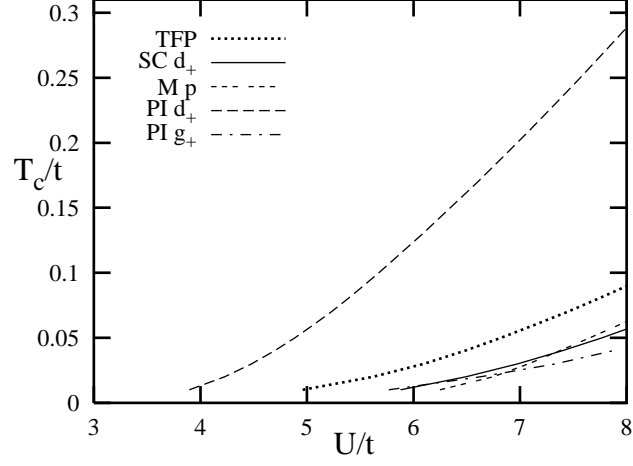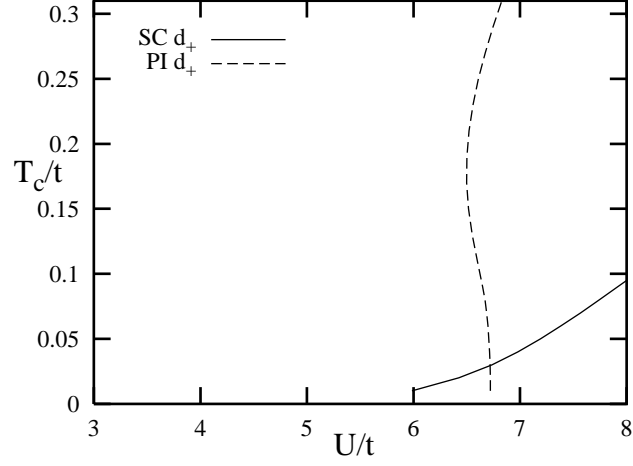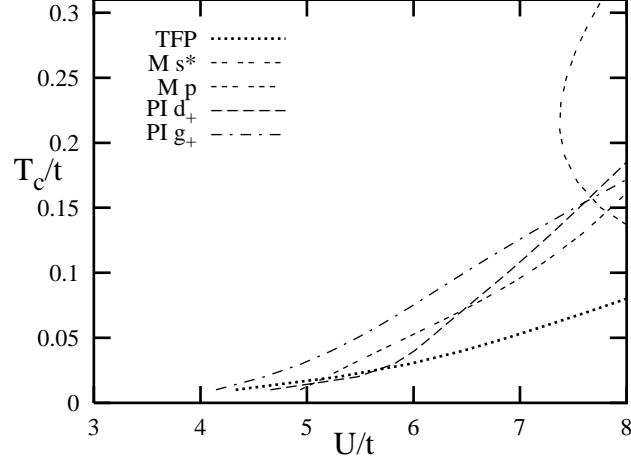
FIG. 3: Temperature phase diagram of the 2D $t - t'$ Hubbard model for $t' = -t/3$, and $n = 0.68$ (the Van Hove filling). Chemical potential varies between $\mu/t = -(1.317 \div 1.339)$. TFP stands for triplet flux phase, M for magnetic particle-hole instability in triplet channel, other notations are the same as in Fig. 1.

FIG. 4: Temperature phase diagram of the 2D $t - t'$ Hubbard model for $t' = -5t/12$, and $n = 0.90$. Chemical potential varies between $\mu/t = -(1.109 \div 0.985)$. Notations are the same as in Fig. 3.

FIG. 5: Temperature phase diagram of the 2D $t - t'$ Hubbard model for $t' = -5t/12$, and $n = 0.55$ (the Van Hove filling). Chemical potential varies between $\mu/t = -(1.666 \div 1.632)$. Notations are the same as in Fig. 3.
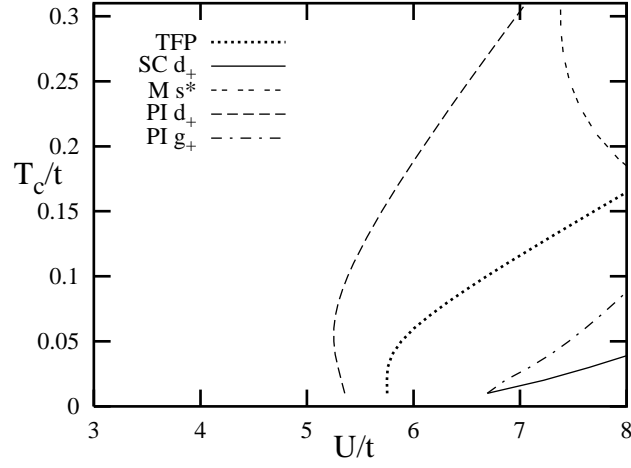

FIG. 6: Temperature phase diagram of the 2D $t - t'$ Hubbard model for $t' = -5t/12$, and $n = 0.70$ (above the Van Hove filling). Chemical potential varies between $\mu/t = -(1.493 \div 1.380)$. Notations are the same as in Fig. 3.
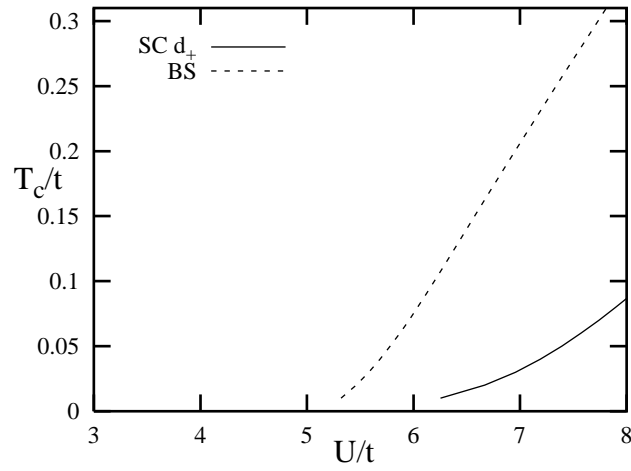

FIG. 7: Temperature phase diagram of the 2D $t - t'$ Hubbard model for $t' = -t/6$, and $n = 1.15$. Chemical potential varies between $\mu/t = -(0.001 \div 0.080)$. Notations are the same as in Fig. 3.
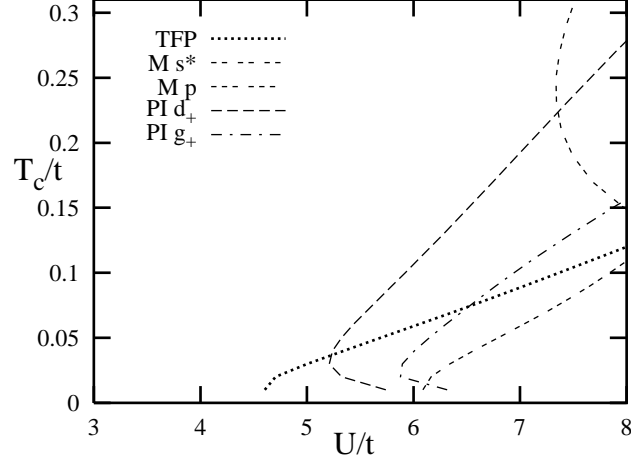
FIG. 8: Temperature phase diagram of the 2D $t - t'$ Hubbard model for $t' = -5t/12$, and $n = 0.60$ (slightly above the Van Hove filling). Chemical potential varies between $\mu/t = -(1.621 \div 1.550)$. Notations are the same as in Fig. 3.
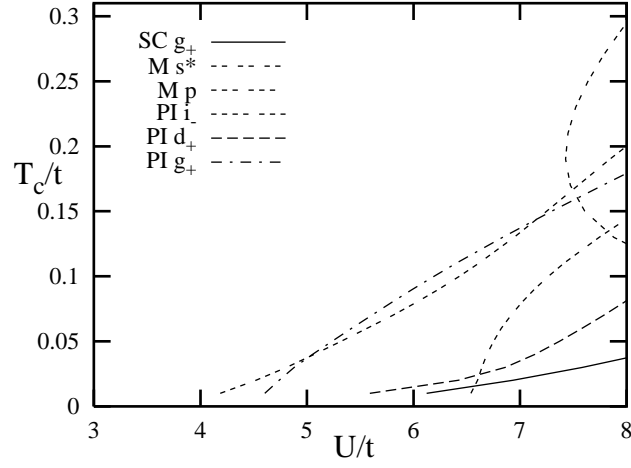

FIG. 9: Temperature phase diagram of the 2D $t - t'$ Hubbard model for $t' = -5t/12$, and $n = 0.50$ (slightly below the Van Hove filling). Chemical potential varies between $\mu/t = -(1.709 \div 1.713)$. Notations are the same as in Fig. 3.
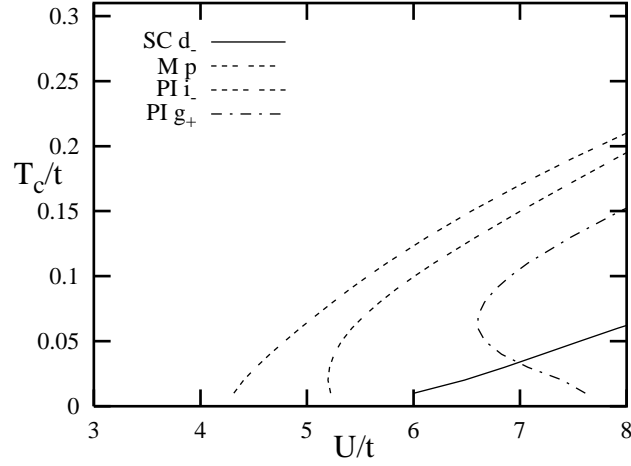

FIG. 10: Temperature phase diagram of the 2D $t - t'$ Hubbard model for $t' = -5t/12$, and $n = 0.35$ (below the Van Hove filling). Chemical potential varies between $\mu/t = -(1.885 \div 1.963)$. Notations are the same as in Fig. 3.